Single-particle dynamics at synchro-betatron coupling resonances

S.Y. Lee
Department of Physics, Indiana University, Bloomington, Indiana 47405
(Received 6 January 1994)

The action-angle variables for the longitudinal motion in synchrotrons are defined to conform with that of the transverse degrees of freedom. The Hamiltonian due to synchro-betatron coupling resonances is formulated in terms of these action-angle variables. A method for the calculation of the synchro-betatron resonance strength is discussed. The dynamics of particle motion near a resonance condition in the presence of nonlinear detuning is studied. The hysteresis phenomena associated with these resonances are discussed and employed to deduce the resonance Hamiltonian from experimental data.

PACS number(s): 41.85.−p, 03.20.+i, 05.45.+b, 29.20.Dh

I. INTRODUCTION

Synchro-betatron coupling resonances (SBRs) are important in electron storage rings and fast cycling proton synchrotrons, where the fractional parts of the synchrotron tune and betatron tunes are of the same order of magnitude. Beam current limitation, beam loss, and performance degradation due to SBR have all been observed in many storage rings [1–9]. This problem is particularly important for high luminosity electron storage rings and for high brightness synchrotron radiation sources.

In the past, many model calculations were performed to estimate effects of SBR [1–14]. In particular, Piwinski and Wrulich [3] pointed out many essential features of the sum and difference SBRs and their driving mechanisms. Similarly, Hamiltonian formalism for the SBR single particle dynamics have been derived by many authors [11–14]. The emittance growth rates due to SBR obtained from the Hamiltonian formalism agree well with numerical simulations [11,12]. More recently, there have also been extensive studies on SBR induced by beam-beam interactions at a crossing angle [13,14]. However, these studies neglect the dependence of tunes on the betatron amplitudes. Since the detuning process is an essential ingredient for the stability of particle motion near a nonlinear resonance, studies of SBR with nonlinear detuning are useful. Because the beam loss mechanism occurs mostly in the transverse degrees of freedom, we will reformulate the SBR Hamiltonian conforming with transverse actions or, equivalently, the Courant-Snyder invariants and study transverse beam dynamics at a SBR.

This paper is organized as follows. In Sec. II, we review the SBR Hamiltonian, where the Panofsky-Wenzel theorem is used to constrain the SBR potential. A method for the calculation of the SBR coupling strength in action-angle variables is discussed. In Sec. III, the dynamics of particle motion near a SBR is studied in the presence of nonlinear detuning parameters. We will show that the nonlinear detuning gives rise to the bifurcation of resonance islands. When the betatron tune is ramped through a resonance, the response will exhibit hysteresis phenomena, which are applied to determine a SBR Hamiltonian from experimental data of tune scan measurements in the large electron-positron (LEP) collider in CERN [9]. The conclusion is given in Sec. IV.

II. THE SBR HAMILTONIAN

The Hamiltonian for a charged particle executing betatron and synchrotron motions in a circular accelerator can be expressed as [11–14]

$$H_0 = H_\perp(x,x',z,z') + H_s\left(\frac{R}{h}\phi, \frac{\Delta p}{p_0}\right), \tag{1}$$

where $H_\perp$ is the Hamiltonian for betatron oscillations with (x,x') for the horizontal and (z,z') for the vertical phase space variables, respectively. The prime represents the derivative with respect to the longitudinal coordinate s along the ring, which serves as the time coordinate. H_s is the Hamiltonian for the synchrotron motion with the conjugate longitudinal phase space coordinates $(\frac{R}{h}\phi, -\frac{\Delta p}{p_0})$, where R is the mean radius of the circular accelerator, h is the harmonic number, ϕ is the rf phase of the particle relative to the synchronous phase angle ϕ_s, and $\frac{\Delta p}{p_0}$ is the momentum deviation of the particle from that of the synchronous particle.

The Hamiltonian for the linearized betatron oscillations is $H_{\perp 0} = \frac{1}{2}(x'^2 + K_x x^2) + \frac{1}{2}(z'^2 + K_z z^2)$, where K_x, K_z are the focusing functions. Similarly, the synchrotron Hamiltonian is given by [11]

$$H_s = -\frac{1}{2}\left(\frac{D_x}{\rho} - \frac{1}{\gamma^2}\right)\left(\frac{\Delta p}{p_0}\right)^2 - \sum_j \frac{eV_j}{h\beta^2 E}[\cos(\phi+\phi_s) + \phi\sin\phi_s]\delta_p(\theta-\theta_j), \tag{2}$$

where D_x is the dispersion function; ρ is the bending radius of dipoles; $\beta c, \gamma$, and E are, respectively, the speed, the Lorentz factor, and the energy of the particle; V_j is

the rf voltage at the θ_j location, and $\delta_p(\theta-\theta_j)$ is the periodic delta function. Since the synchrotron oscillation is relatively slow, the synchrotron Hamiltonian averaged over one revolution becomes

$$\langle H_s\rangle = -\frac{1}{2}\eta\left(\frac{\Delta p}{p_0}\right)^2 - \frac{\nu_s^2}{h^2|\eta|}[\cos(\phi+\phi_s)-\cos\phi_s+\phi\sin\phi_s], \quad (3)$$

where $\nu_s=\sqrt{\frac{h|\eta|eV}{2\pi\beta^2E}}$ is the synchrotron tune of a stationary bucket at small synchrotron amplitudes with V as the effective voltage of the entire ring and a constant was added in Eq. (3) to shift the Hamiltonian value.

The actions of the synchrotron and the linearized betatron oscillations are defined as

$$I_s=\frac{R}{2\pi h}\oint\frac{\Delta p}{p_0}d\phi, \quad I_x=\frac{1}{2\pi}\oint x'dx, \quad I_z=\frac{1}{2\pi}\oint z'dz.$$

The transverse actions are also called the Courant-Snyder invariants. Table I lists parameters of some electron storage rings and the ratio $\frac{I_s}{I_x}$ of rms actions. Appendix A discusses general properties of I_s and Appendix B examines scaling properties of the longitudinal and transverse actions. Note here that the ratio of $\frac{I_s}{I_x}$ is about 50–200 for high energy colliders, which does not minimize the transverse emittance. On the other hand, the ratio is about 600–700 for synchrotron radiation sources, which minimize the transverse emittances. However, the large ratio for synchrotron radiation sources arises mainly from their small synchrotron tunes. Had the synchrotron tunes of the Advanced Photon Source (APS) and the Advanced Light Source (ALS) increased by a factor of 10, the ratio would have been decreased by the same factor.

Transforming the coordinate system onto the action-angle variables and using the orbital angle θ for time coordinate, one obtains the unperturbed Hamiltonian as

$$H_0=\nu_xI_x+\nu_zI_z+\frac{1}{2}\alpha_{xx}I_x^2 +\alpha_{xz}I_xI_z+\frac{1}{2}\alpha_{zz}I_z^2+E_s(I_s), \quad (4)$$

where ν_x,ν_z are the horizontal and vertical betatron tunes and the nonlinear detuning parameters α_{xx},α_{xz}, and α_{zz} (due mainly to sextupoles, octupoles, and beam-beam interactions in storage rings and colliders) are the order of 10^3-10^4 m^{-1}. It is worth pointing out that the perturbation expansion in power series of I_x,I_z may not be appropriate for the nonlinear detuning due to beam-beam interactions, where the tune shifts for particles at large amplitudes are small.

The Hamiltonian value of the longitudinal motion, $E_s(I_s)$, can be expanded as (see Appendix A)

$$E_s(I_s)=-\frac{\eta}{|\eta|}(Q_sI_s+\tfrac{1}{2}\alpha_{ss}I_s^2), \quad (5)$$

where $Q_s=\nu_s|\cos\phi_s|^{1/2}$. The detuning parameter $\alpha_{ss}=-\frac{h^2|\eta|}{8R}(1+\frac{5}{3}\tan^2\phi_s)$, tabulated in Table I, is of the order of -10 m^{-1}, which is normally much smaller than the betatron detuning parameters.

A. The SBR potential

The SBR potential $V_{\rm SBR}$ may arise from dispersion functions in rf cavity locations, transverse fields with lon-

TABLE I. Parameters of some electron storage rings. The action listed in this table is the action for the rms particle. The symbols for storage rings are as follows: BEPC, Beijing electron positron collider; CESR, Cornell; LER, low energy SLAC B factory; HER, high energy SLAC B factory; LEP, CERN; APS, advanced photon source at Argonne; ALS, advanced light source at LBL.

Parameter	BEPC	CESR	LER (e^+)	HER (e^-)	LEP	APS	ALS
E (GeV)	2.2	6	3.1	9	55	7	1.5
ν_x	5.8	9.38	32.28	25.28	76.2	35.22	14.28
ν_z	6.8	9.36	35.18	24.18	70.2	14.3	8.18
ϵ_x (nm)[a]	450	240	96	48	51	8	4.8
ϵ_z (nm)	35	8	3.86	1.93	0.51	0.08	0.48
ρ (m)	10.35	60	30.6	165.0	3096.2	38.96	4.01
$10^4\alpha$	400	152	14.9	24.4	3.866	2.374	14.3
C (m)	240.4	768.4	2199.3	2199.3	26658.9	1060	196.8
h	160	1281	3492	3492	31320	1248	328
$f_{\rm rf}$ (MHz)	199.5	499.8	476	476	352.2	352.96	499.65
ν_s	0.016	0.064	0.0498	0.0522	0.085	0.0066	0.0082
$10^4\,\frac{\Delta E}{E_0}$	4.0	6.3	9.5	6.1	8.4	9.6	7.1
$\mathcal{A}$ (10^{-4} eV s)	3.5	7.2	3.1	5.7	78.	4.1	0.43
I_s (10^3nm)	7.7	5.7	4.7	3.0	6.8	2.8	1.4
$\frac{I_s}{I_x}$	34	48	98	127	267	699	574
α_{ss} (m^{-1})[b]	-3.3	-25.5	-6.5	-10.6	-11.2	-0.27	-0.61
$\hat{\phi}_c$ (10^{-4}rad)	8.0	11.1	1.4	2.4	1.6	1.3	2.8

[a]The rms action is $I_x=\frac{\epsilon_x}{2}=\frac{1}{2}\frac{\sigma_x^2}{\beta_x}$.

[b]This table calculates only the nonlinear detuning for $\phi_s=0$ or π. The actual longitudinal nonlinear detuning parameter can be about 10% larger depending on the value of ϕ_s.

gitudinal variation, dipole field modulation at dispersive locations, beam-beam interactions with a nonzero crossing angle, etc. [1–14]. The resonance strength should be calculated from all possible sources.

In general, the SBR potential must satisfy the Panofsky-Wenzel theorem, which relates the transverse kicks to the longitudinal energy gain. Consider a particle of charge e and velocity $\vec{v} = \frac{d\vec{s}}{dt}$ experiencing a kick from a component in an accelerator. The total momentum change is given by

$$\Delta\vec{p} = e\int_{t_a}^{t_b}(\vec{E} + \vec{v}\times\vec{B})dt,$$

where $\vec{E}, \vec{B}$ are electromagnetic fields and $t_b - t_a$ is the transit time of the kicker component. The total energy change will be

$$\Delta E = e\int_{s_a}^{s_b}\vec{E}\cdot d\vec{s},$$

where s_a, s_b are the entrance and exit azimuthal coordinates of the kicker. Then the Panofsky-Wenzel theorem yields a relation between the transverse kick and the energy gain [17], i.e.,

$$\frac{h}{R}\frac{\partial}{\partial\phi}\left(\frac{\Delta p_\perp}{p_0}\right) = \nabla_\perp\left(-\frac{\Delta E}{\beta^2 E_0}\right), \tag{6}$$

where $\frac{\Delta p_\perp}{p_0}$ is the transverse kick, $\frac{R}{h}\phi$ is the longitudinal phase space coordinate of the particle, and $\nabla_\perp$ is the transverse gradient. Thus if the transverse kick depends on the longitudinal coordinates, then the energy gain will also depend on the transverse coordinates.

This SBR potential, which satisfies the Panofsky-Wenzel theorem, can generally be expressed as a function of six-dimensional (6D) phase space coordinates. Because of the periodic nature of a circular accelerator and the quasiharmonic nature of synchrotron and betatron oscillations, the SBR potential can be expanded as [15]

$$V_{\rm SBR} = \sum_{m_x,m_z,m_s,\ell} g_{\bar{m},\ell}(I_x, I_z, I_s)e^{i(m_x\psi_x + m_z\psi_z + m_s\psi_s - \ell\theta)}, \tag{7}$$

where m_x, m_z, m_s, and ℓ are integers and $\bar{m}$ represents (m_x, m_z, m_s). The SBR coupling strength $g_{\bar{m},\ell}$ is given by the inverse Fourier transform of the SBR potential, i.e.,

$$g_{\bar{m},\ell} = \frac{1}{(2\pi)^4}\int V_{\rm SBR}e^{-i(m_x\psi_x + m_z\psi_z + m_s\psi_s - \ell\theta)} \times d\psi_x d\psi_z d\psi_s d\theta, \tag{8}$$

which scales generally as $I_x^{\frac{|m_x|}{2}} I_z^{\frac{|m_z|}{2}} I_s^{\frac{|m_s|}{2}}$.

1. The SBR potential due to nonzero dispersion in rf cavities

The most common SBR arises from nonzero dispersion functions at rf cavity locations. The SBR potential due to dispersion in rf cavities is given by [11]

$$V_{\rm SBR} = -R\sum_j \frac{eV_j}{h\beta^2 E}[\cos(\phi + \phi_s + \phi_c) - \cos(\phi + \phi_s) + \phi_c\sin\phi_s]\delta_p(\theta - \theta_j), \tag{9}$$

where the phase shift ϕ_c due to the synchro-betatron coupling is

$$\phi_c = -\frac{h}{R}(D_x x' - D_x' x) = \frac{2h}{R}\sqrt{I_x I_D}\sin(\mu_x - \mu_D). \tag{10}$$

Here (I_x, μ_x) are the action and phase of betatron oscillations and (I_D, μ_D) are the dispersion action and dispersion phase [16], i.e.,

$$D_x = \sqrt{2\beta_x I_D}\cos\mu_D,$$
$$\beta_x D_x' - \frac{1}{2}\beta_x' D_x = -\sqrt{2\beta_x I_D}\sin\mu_D\ .$$

Note here that I_D and $\mu_x - \mu_D$ are constant in a straight section without dipoles. Therefore, the rf phase shift ϕ_c is constant for rf cavities located in a straight section. The contribution from all cavities in a straight section to $V_{\rm SBR}$ is an arithmetic sum. Varying the phase advance within a straight section does not alter the SBR strength.

Since the dispersion action is generally proportional to $\rho\theta_d^3$, where θ_d is the bending angle of dipoles in a half cell, we define $\hat{\phi}_c$ as the maximum phase shift parameter as

$$\hat{\phi}_c = \frac{2h}{R}\sqrt{I_{x,\rm rms}\rho\theta_d^3}.$$

Table I lists $\hat{\phi}_c$ for some storage rings. In reality, the actual phase shift ϕ_c can be one order of magnitude smaller than $\hat{\phi}_c$ because the actual dispersion action at the rf cavity locations is small. We note, however, that $\hat{\phi}_c$ for the Cornell Electron-Positron Storage Ring (CESR) and the Beijing Electron Positron Collider are much larger than other storage rings. This is due to their smaller circumferences and large rms betatron actions. It remains to be verified that these two colliders are much more sensitive to SBR. Incidentally, the $\hat{\phi}_c$ parameter for the Stanford Positron Electron Accelerator Ring (SPEAR) at the Stanford Linear Accelerator Center (SLAC) equals that of CESR.

The SBR potential of Eq. (9) can then be written as

$$V_{\rm SBR} = -R\sum_j \frac{eV_j}{h\beta^2 E}\{[\cos(\phi + \phi_s)(\cos\phi_c - 1)] - [\sin(\phi + \phi_s)\sin\phi_c - \phi_c\sin\phi_s]\}\delta_p(\theta - \theta_j), \tag{11}$$

which satisfies the Panofsky-Wenzel theorem. The coupling strength $g_{\bar{m},\ell}$ can be obtained easily from the inverse Fourier transformation of Eq. (8). To perform betatron phase integrals, the betatron phase μ_x should be replaced by $\psi_x + \mu_x - \nu_x\theta$, where ψ_x is the conjugate phase variable to the action I_x. To perform the synchrotron phase integrals, a coordinate transformation discussed in Appendix A becomes handy. The first square bracket term in Eq. (11) contributes to even m_x in Eq. (8), while

the second square bracket term gives rise to odd m_x. Because ϕ_c is relatively small, $|m_x| > 1$ is usually less important. On the other hand, the synchrotron amplitude σ_ϕ is of the order of 0.2 rad. Thus high order synchrotron sidebands with $|m_s| > 1$ can be important.

2. *The SBR potential arising from transverse kicks with longitudinal dependence*

Any differentiable function of $(x, z, \frac{R}{h}\phi)$, e.g., $f(x, z, \frac{R}{h}\phi)$, that satisfies the Panofsky-Wenzel theorem can be used for the SBR potential. Since the electromagnetic fields in transverse kicker components can be expanded in Taylor series, the SBR potential can be expressed as

$$V_{\rm SBR} = -\left(\frac{R}{h}A_z z\phi + \frac{R}{h}A_x x\phi + \cdots\right)\delta_p(\theta - \theta_i). \quad (12)$$

Here the coefficients $A_{x,z}$ are given by the transverse gradients of the integrated change of $-\frac{\Delta p}{p_0}$ in a kicker component, i.e., $A_x = \frac{\partial}{\partial x}[-\Delta(\frac{\Delta p}{p_0})]$, etc.

The beam-beam interaction at a nonzero crossing angle is another example of transverse kick, which may depend on the longitudinal coordinate. Using the the Panofsky-Wenzel theorem, the SBR potential arising from the beam-beam interaction, at a horizontal crossing angle of $2\theta_x$, can be written generally as

$$V_{\rm bb,SBR} = -\left[U\left(x + \theta_{\rm x}\frac{R}{h}\phi, z, \theta\right) - U(x, z, \theta)\right], \quad (13)$$

where $U(x, z, \theta)$ is the beam-beam potential. A commonly used Gaussian beam-beam potential model is given by [6,13,14]

$$U(x, z, \theta) = \frac{N_B r_0}{\gamma}\int_0^\infty \frac{1 - \exp\left(-\frac{x^2}{2\sigma_x^2+w} - \frac{z^2}{2\sigma_z^2+w}\right)}{(2\sigma_x^2 + w)^{1/2}(2\sigma_z^2 + w)^{1/2}}dw \times\delta_p(\theta - \theta_i), \quad (14)$$

where N_B is the number of particles per bunch, r_0 is the classical radius of the particle, and σ_x, σ_z are the rms horizontal and vertical beam sizes.

Because nonzero crossing angles in beam-beam interactions may give rise to SBR, high energy colliders are usually designed with zero crossing angle. However, when the number of bunches is increased in order to gain necessary luminosity, parasitic crossings do occur. Because the parasitic crossing angle is usually not zero, it is possible that the long range beam-beam interactions can also drive SBR. Detailed analysis of such a mechanism may be important.

III. BEAM DYNAMICS NEAR A SBR

Following the discussion in Sec. II, the SBR Hamiltonian for a particle in a circular accelerator can generally be represented by

$$H = H_0(I_x, I_z, I_s) + \sum_{m_x,m_z,m_s,\ell} g_{\vec{m},\ell}(I_x, I_z, I_s)e^{i(m_x\psi_x + m_z\psi_z + m_s\psi_s - \ell\theta)}, \quad (15)$$

where H_0 is the unperturbed Hamiltonian shown in Eq. (4). In a single resonance dominant regime at the following resonance condition:

$$m_x\nu_x + m_z\nu_z - \frac{\eta}{|\eta|}m_s Q_s = \ell, \quad (16)$$

the Hamiltonian can be approximated by

$$H \approx H_0 + |g_{\vec{m},\ell}|\cos(m_x\psi_x + m_z\psi_z + m_s\psi_s - \ell\theta + \gamma_{\vec{m},\ell}). \quad (17)$$

It is easy to show that the Hamiltonian of Eq. (17) has two invariants, i.e.,

$$m_s I_x - m_x I_s = \text{const}, \qquad m_s I_z - m_z I_s = \text{const}. \quad (18)$$

These invariants define a line in the (I_x, I_z, I_s) action space. The variation of actions becomes

$$\Delta I_x = \frac{m_x}{m_s}\Delta I_s, \quad \Delta I_z = \frac{m_z}{m_s}\Delta I_s. \quad (19)$$

Since the rms longitudinal action I_s of a beam is much larger than the corresponding rms actions of the transverse planes, the percentage increase in transverse actions is much larger as shown in Eq. (19) for *both* sum and difference SBRs. Since storage rings are usually operating close to the transverse dynamical aperture limit, particle loss appears dominantly in transverse degrees of freedom. This loss mechanism has been observed in PETRA and DORIS [6], in CESR [7], and during the injection in LEP [8]. Based on $I_s \gg I_{x,z}$, approximate treatment of SBRs will be discussed as follows.

A. Approximate treatment for $\nu_x \pm m_s Q_s = \ell$ resonances

Since $I_x \ll I_s$ for most of particles in the bunch, the percentage variation of the longitudinal action is small. We can thus approximate $g = \tilde{g}I_x^{1/2}$ for $\nu_x \pm m_s Q_s = \ell$ SBR, where $\tilde{g}$ depends on m_s, I_s, and ℓ. The Hamiltonian near the first order sideband resonance can be expressed as

$$H = \nu_x I_x + \frac{1}{2}\alpha_{xx}I_x^2 - \frac{\eta}{|\eta|}(Q_s I_s + \tfrac{1}{2}\alpha_{ss}I_s^2) + \tilde{g}I_x^{1/2}\cos(\psi_x + m_s\psi_s - \ell\theta + \gamma). \quad (20)$$

Using the generating function

$$F_2 = (\psi_x + m_s\psi_s - \ell\theta + \gamma)I_1 + \psi_s I_2,$$

the Hamiltonian in the resonance rotating frame becomes $H = H_1(I_1, \psi_1, I_2) + H_2(I_2)$, with $H_2(I_2) = -\frac{\eta}{|\eta|}(Q_s I_2 +$

$\frac{1}{2}\alpha_{ss}I_2^2$) and

$$H_1 = \delta_1 I_1 + \frac{1}{2}\alpha_1 I_1^2 + \tilde{g} I_1^{1/2}\cos\psi_1. \tag{21}$$

Here $\delta_1 = \nu_x - \frac{\eta}{|\eta|}m_s(Q_s + \alpha_{ss}I_2) - \ell$ is the resonance proximity parameter, $\alpha_1 = \alpha_{xx} - \frac{\eta}{|\eta|}m_s^2\alpha_{ss}$ is the effective resonance detuning parameter, $I_1 = I_x$, and $I_2 = I_s - m_s I_x$.

Because of the fact that $I_s \gg I_x$, the approximate SBR Hamiltonian in the resonance rotating frame is identical to that of the first order parametric resonance system [18]. Hamilton's equations of motion are given by

$$\dot{\psi}_1 = \delta_1 + \alpha_1 I_1 + \frac{1}{2}\tilde{g} I_1^{-1/2}\cos\psi_1, \quad \dot{I}_1 = \tilde{g} I_1^{1/2}\sin\psi_1. \tag{22}$$

The equation for fixed points of the Hamiltonian is given by

$$w^3 - bw + \frac{1}{2}a = 0, \tag{23}$$

with

$$w = I_1^{1/2}\cos\psi_1 \ (\psi_1 = 0 \text{ or } \pi), \quad b = -\frac{\delta_1}{\alpha_1}, \quad a = \frac{\tilde{g}}{\alpha_1}.$$

First, we examine the trivial case with $\alpha_1 = 0$. The fixed point is located at $w_{\rm FP} = -\frac{\tilde{g}}{2\delta_1}$. The condition for minimizing effects of SBR becomes $|w_{\rm FP}| < \frac{1}{2}\sqrt{I_{1,\rm rms}}$ or, equivalently, $|\delta_1| > \frac{|\tilde{g}|}{\sqrt{I_{1,\rm rms}}}$.

When the nonlinear detuning is not zero, solutions of Eq. (23) are well known [18]. If the resonance proximity parameter b is larger than or equal to a bifurcation value b_b, given by

$$b_b = 3\left(\frac{a}{4}\right)^{2/3}, \tag{24}$$

there are three solutions to Eq. (23) given by

$$\begin{aligned} w_1(b) &= -\frac{2}{\sqrt{3}}b^{1/2}\cos\frac{\xi}{3}, \\ w_2(b) &= \frac{2}{\sqrt{3}}b^{1/2}\sin\left(\frac{\pi}{6} - \frac{\xi}{3}\right), \\ w_3(b) &= \frac{2}{\sqrt{3}}b^{1/2}\sin\left(\frac{\pi}{6} + \frac{\xi}{3}\right). \end{aligned} \tag{25}$$

Here $\xi = \arctan\sqrt{(\frac{b}{b_b})^3 - 1}$, with $\frac{b}{b_b} \geq 1$. The solutions w_1 with $\psi_1 = \pi$ and w_2 with $\psi_1 = 0$ are stable fixed points (SFPs) and the solution w_3 with $\psi_1 = 0$ is the unstable fixed point (UFP). Stable tori in phase space are closed curves around the SFPs. The particle motion in phase space can be described by the tori of constant Hamiltonian H_1 around SFPs (see [18]).

When $b < b_b$, there is only one real solution to Eq. (23) given by

$$w_1 = -\left(\frac{a}{4}\right)^{1/3}\left\{\left[\sqrt{1 - \left(\frac{b}{b_b}\right)^3} + 1\right]^{1/3} - \left[\sqrt{1 - \left(\frac{b}{b_b}\right)^3} - 1\right]^{1/3}\right\}, \tag{26}$$

and all tori are closed curves orbiting about the outer SFP. The condition for minimizing the effects of SBR can be analyzed similar to that of rf phase modulation [18]. In particular, when $b = b_b$, the SFP becomes

$$w_1 = -\left(\frac{2\tilde{g}}{\alpha_1}\right)^{1/3}.$$

To ascertain small perturbations to the beam distribution, the SFP must be near the bunch center, i.e., $|w_1|^2 \leq \frac{1}{2}I_{1,\rm rms}$. This means that the resonance strength should be $|\tilde{g} I_{1,\rm rms}^{1/2}| \leq \frac{1}{2^{5/2}}|\alpha_1 I_{1,\rm rms}^2|$, if the SBR resonance is located at $\delta_1 = -\frac{3}{2^{4/3}}\alpha_1^{1/3}\tilde{g}^{2/3}$.

Beyond the bifurcation tune, i.e., the resonance proximity parameter $b > b_b$, the SBR resonance island bifurcates into two stable islands. At a resonance strength where both SFPs are within the dynamical aperture of the accelerator, a beam can split into two beamlets in the betatron phase space. These two beamlets are orbiting about the closed orbit at the tune of $\nu_x \pm m_s Q_s - \ell$. A high resolution profile monitor may be able to resolve these islands. However, since the beam bunch is composed of particles with all synchrotron and betatron phases, the actual island is a ring of islands in the betatron phase space.

When the betatron tune is ramped through the resonance, these islands may exhibit hysteresis phenomena. At a betatron tune with $b \ll b_b$, the equilibrium bunch center is located at the only SFP given by Eq. (26). When the tune is ramped so that b is approaching b_b from below, the amplitude of SFP increases and the bunch follows adiabatically with the outer SFP, beyond the bifurcation point b_b, until the outer island becomes too small. The beam bunch will jump from the outer island into the inner island.

On the other hand, at a betatron tune with $b \gg b_b$, the equilibrium centroid of the beam bunch is located at the inner SFP of Eq. (25), because the outer island is either nonexistent or very small. When the tune is ramped so that b is approaching b_b from above, the beam will follow the inner SFP until the separatrix cuts through the center of the phase space. Then each particle in the beam bunch will perform large amplitude oscillations about its corresponding outer SFP. These hysteresis phenomena have been observed in synchrotron motion with rf phase modulation [18]. The SBR Hamiltonian can be determined from the measured hysteresis curves. In the following, we discuss an example of deducing SBR Hamiltonian from the data of tune scan experiments in LEP [9].

1. Experimental observation of SBR in LEP

Recently, experimental measurements of beam size as a function of the horizontal betatron tune across the

$\nu_x - 2Q_s = \ell$ resonance were performed in LEP [9]. The upper two panels of Fig. 1 show the rms beam sizes vs the horizontal betatron tune, which was scanned from 0.1 to 0.3 while the vertical tune was 0.20 and the synchrotron tune was 0.076. The rms beam sizes obtained from downward tune scan were shown upside down to exhibit possible asymmetry between the upward and the downward tune scans.

The increase in beam size at $\nu_x \approx 0.152$ might result from the SBR at $\nu_x - 2Q_s = \ell$. The difference between the upward and the downward scans may result from the hysteresis phenomena discussed in the preceding section. The lowest panel of Fig. 1 shows $\sqrt{\beta_x I_{x,\mathrm{SFP}}}$ deduced from the data along with the fit of the model discussed in the preceding section. In the following, I will discuss the model for deducing SFPs from experimental data. However, one should take the following model-dependent analysis with a grain of salt.

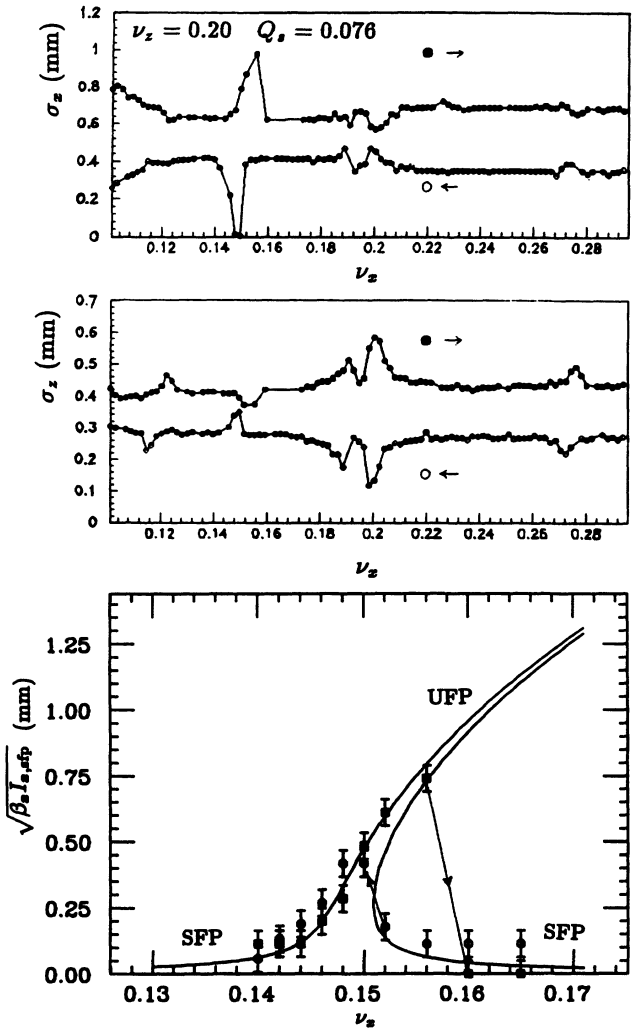

FIG. 1. The rms beam sizes, with resolution of about 0.05 mm, obtained from tune scan measurements in LEP are shown as a function of the horizontal tune in the top two panels [9]. The synchrotron and the vertical tunes were kept constant at 0.076 and 0.20, respectively. The lowest panel shows the SFP amplitudes, i.e., $\sqrt{\beta_x I_{x,\mathrm{SFP}}}$, derived from experimental data. The solid squares correspond to data from the upward tune ramp and the circles correspond to data from the downward tune ramp. An error of 0.1 mm was assigned to reflect the 10% variation in our derived Hamiltonian parameters. Smooth curves are solutions of Eq. (23) fitted with parameters $Q_{s,\mathrm{eff}} = 0.074$, $\alpha_1 = -1.4 \times 10^4 \beta_x$ m^{-1} and $|\tilde{g}| = \frac{1.0}{\sqrt{\beta_x}} \times 10^{-6}$ m$^{1/2}$. This model does not explain why σ_z decreases during resonance crossing.

We first realize that SFPs and the UFP of the first order resonance are smooth curves shown in the lowest panel of Fig. 1 (see also [18]). When the betatron tune is ramped upward, toward the resonance frequency, the outer SFP and its island move outward in the betatron phase space. The center of the beam bunch follows adiabatically the outer SFP of the solution w_1 in the preceding section. The measured beam size is given by (quadrature assumption)

$$\sigma^2_{\mathrm{measured}} = \beta_x I_{x,\mathrm{SFP}} + \beta_x \epsilon_x, \tag{27}$$

where $\sqrt{\beta_x \epsilon_x}$ is the off-resonance beam size and $I_{x,\mathrm{SFP}}$ is the rms action of the SFPs of all particles, shown as solid square symbols in Fig. 1. When the tune is ramped upward, the center of the beam bunch follows the SFP outward and beyond the bifurcation tune, until the outer island size becomes too small to contain the bunch. The beam bunch then jump from the outer SFP to the inner SFP shown as a downward arrow in Fig. 1.

On the other hand, when the betatron tune is ramp downward toward the resonance tune, the beam would stay with the inner stable island, which is usually at a very small betatron amplitude. The inner SFPs shown as open circles in Fig. 1 can be obtained from experimental data similar to that of Eq. (27). The response of the beam size to the tune change will be small until the separatrix cuts through the origin. Then the beam bunch would orbit about the outer SFP at twice the SFP amplitude. This transient effect has been observed [18]. Thus the measured SFP, shown as open circle in the lower part of Fig. 1 for $b < b_b$, is given by

$$\sqrt{\beta_x I_{x,\mathrm{SFP}}} = \frac{1}{2}\sqrt{\sigma^2_{\mathrm{measured}} - \beta_x \epsilon_x}. \tag{28}$$

It is worth mentioning that the response observed at the bifurcation point during the downward tune ramp may depend on the ramping speed and the radiation damping rate. If the radiation damping rate is faster than the tune ramp measurement rate, then the factor of $\frac{1}{2}$ in Eq. (28) should be replaced by 1. In both cases, the data will exhibit hysteresis phenomena. However, if the tune ramp measurement rate is slower than the rate of quantum fluctuation, which characterizes the rate that beam particles can jump from one island to the other due to quantum fluctuation, then the hysteresis phenomena may disappear. In the present analysis, we have assumed a fast tune ramp measurement rate and a small quantum fluctuation rate.

The deduced parameters are $Q_{s,\mathrm{eff}} = 0.074 \pm 0.0005$, $\alpha_1 = -1.4 \times 10^4 \beta_x$ m^{-1}, and $|\tilde{g}| = \frac{1.0}{\sqrt{\beta_x}} \times 10^{-6}$ m$^{1/2}$, where β_x m is the betatron amplitude function at the location of profile monitor. Because of the uncertainty in the data analysis, we assign an error bar of 0.1 mm in

$\sqrt{\beta_x I_{x,\mathrm{SFP}}}$ which reflects 10% variation in our deduced parameters α_1 and $\tilde{g}$. The SBR Hamiltonian is therefore only determined up to a scaling factor. Calculations and measurements of machine parameters, such as α_{xx}, β_x, etc., can be used to confirm the validity of the model for data analysis. It is possible to formulate a more sophisticated model by making ensemble sum of particle motion with a given distribution function. For simplicity, I defer these detailed studies to the future. Similar analyses for tune ramp measurements at $\nu_z - 2Q_s$ and $\nu_z - 3Q_s$ can be performed to test the consistency of the present model. The source for the vertical SBR may be determined from these data analyses.

B. The $2\nu_x \pm m_s Q_s = \ell$ SBR resonances

Near a $2\nu_x \pm m_s Q_s = \ell$ SBR resonance, the Hamiltonian can be approximated as

$$H = \nu_x I_x + \tfrac{1}{2}\alpha_{xx} I_x^2 - \frac{\eta}{|\eta|}(Q_s I_s + \tfrac{1}{2}\alpha_{ss} I_s^2) + \tilde{g} I_x \cos(2\psi_x + m_s \psi_s - \ell\theta + \gamma). \quad (29)$$

Using the generating function

$$F_2 = \left(\psi_x + \frac{m_s}{2}\psi_s - \frac{\ell}{2}\theta + \frac{\gamma}{2}\right) I_1 + \psi_s I_2,$$

the Hamiltonian in the resonance rotating frame becomes $H = H_1(I_1, \psi_1, I_2) + H_2(I_2)$, with $H_2(I_2) = -\frac{\eta}{|\eta|}(Q_s I_2 + \frac{1}{2}\alpha_{ss} I_2^2)$ and

$$H_1 = \delta_1 I_1 + \frac{1}{2}\alpha_1 I_1^2 + \tilde{g} I_1 \cos 2\psi_1, \quad (30)$$

which is identical to that of the second order parametric resonance system [19]. Here $\delta_1 = \nu_x - \frac{\eta}{|\eta|}\frac{m_s}{2}(Q_s + \alpha_{ss} I_2) - \frac{\ell}{2}$ is the resonance proximity parameter, $\alpha_1 = \alpha_{xx} - \frac{\eta}{|\eta|}\frac{m_s^2}{4}\alpha_{ss}$ is the effective resonance detuning parameter, $I_1 = I_x$, and $I_2 = I_s - \frac{m_s}{2} I_x$. Hamilton's equations of motion are given by

$$\dot{\psi}_1 = \delta_1 + \alpha_1 I_1 + \tilde{g}\cos 2\psi_1, \quad \dot{I}_1 = 2\tilde{g} I_1 \sin 2\psi_1. \quad (31)$$

In the case of zero detuning, i.e., $\alpha_1 = 0$, the constant Hamiltonian flow is given by

$$H_1 = \delta_1 I_1 + \tilde{g} I_1 \cos 2\psi_1 = E_1.$$

Let us define $X = \sqrt{I_1}\cos\psi_1, P = \sqrt{I_1}\sin\psi_1$. The Hamiltonian flow is given by

$$(\delta + \tilde{g})X^2 + (\delta_1 - \tilde{g})P^2 = E_1. \quad (32)$$

Thus when $|\delta_1| \le |\tilde{g}|$, the Hamiltonian flow becomes hyperbolic, which gives rise to large betatron oscillations bounded only by the conservation law of I_2 = constant. Because $I_s \gg I_x$, particle loss would occur. When $|\delta| > |\tilde{g}|$, the Hamiltonian flow is elliptical. The stability of particle motion therefore requires $|\delta_1| \gg |\tilde{g}|$.

When the detuning parameter is not zero, the fixed points are given by

$$I_{1,\mathrm{SFP}} = \begin{cases} 0 & \text{if } \frac{\delta_1}{\alpha_1} > |\frac{\tilde{g}}{\alpha_1}|, \quad \frac{\delta_1}{\alpha_1} < -|\frac{\tilde{g}}{\alpha_1}| \\ -\frac{\delta_1}{\alpha_1} + |\frac{\tilde{g}}{\alpha_1}| & \text{if } \frac{\delta_1}{\alpha_1} \le |\frac{\tilde{g}}{\alpha_1}|, \end{cases}$$

$$I_{1,\mathrm{UFP}} = \begin{cases} 0 & \text{if } |\frac{\delta_1}{\alpha_1}| \le |\frac{\tilde{g}}{\alpha_1}| \\ -\frac{\delta_1}{\alpha_1} - |\frac{\tilde{g}}{\alpha_1}| & \text{if } \frac{\delta_1}{\alpha_1} \le -|\frac{\tilde{g}}{\alpha_1}|. \end{cases}$$

Figure 2 shows the relation of the $|\frac{\alpha_1}{\tilde{g}}| I_{1,\mathrm{SFP}}$ and $|\frac{\alpha_1}{\tilde{g}}| I_{1,\mathrm{UFP}}$ as a function of $\zeta = \frac{\alpha_1}{|\alpha_1|}\frac{\delta_1}{\tilde{g}}$. The bifurcation of resonance islands occurs at $\zeta = 1$ and -1. To ensure small SBR effect on the beam, $\zeta > 1$ and $\zeta \ll \zeta_c$, where the parameter ζ_c is determined from the condition that the UFP of the Hamiltonian is outside the betatron beam width. If the resonance strength is small so that the SFPs are located inside the dynamical aperture, then the beam bunch will split into two or three beamlets in the betatron phase space. These beamlets are rotating in betatron phase space at the tune of $\nu_x \pm \frac{1}{2}m_s Q_s - \frac{\ell}{2}$.

Experimental measurements of $2\nu_z - 2Q_s = \ell$ at CESR Cornell (see Fig. 3 of Ref. [7]) showed that the vertical beam size was increased by a factor of about 10%. Here we assume that the measured beam size is the equilibrium beam distribution in the presence of the nonlinear detuning and a weak SBR resonance. In the region of the tune space $|\delta_1| \le |\tilde{g}|$, the beam distribution resembles the shape of a dumbbell in the betatron phase space. (Since a beam bunch is composed of particles of different betatron and synchrotron phases, the actual beam distribution is an O-ring in this case.) The maximum beam size should correspond to the maximum width of the dumbbell with $I_{\mathrm{SFP}} = 2|\frac{\tilde{g}}{\alpha}|$ at $\delta_1 = -\alpha\frac{|\tilde{g}|}{|\alpha|}$. Thus the ratio of beam size is given by

$$\sqrt{\frac{\hat{I}_{\mathrm{SFP}} + \epsilon_z}{\epsilon_z}} \approx 1.1,$$

where ϵ_z is the intrinsic beam emittance of the beam and

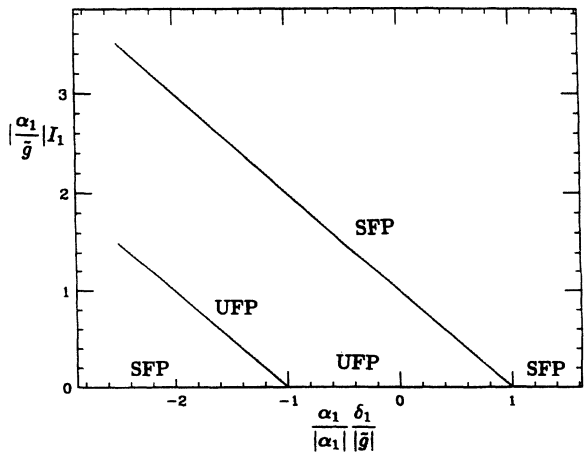

FIG. 2. The actions of SFPs and UFPs divided by a normalized resonance strength for the second order SBR are plotted as a function of the normalized resonance proximity parameter.

the factor of 1.1 is obtained from Fig. 3 of Ref. [7]. Thus we obtain $\hat{I}_{\rm SFP} \approx 2|\frac{\tilde{g}}{\alpha_1}| \approx 0.2\epsilon_z$. This estimation gives only the ratio of the resonance strength to the nonlinear detuning parameter. To measure all parameters for the SBR Hamiltonian, ramped tune measurements to observe hysteresis phenomena would be very helpful.

When the betatron tune is ramped such that ζ is decreasing from above 1, the rms beam size will increase according to $\sqrt{\beta_z(\epsilon_z + I_{\rm SFP})}$ shown in Fig. 2. The rms beam size will continue to increase beyond the second bifurcation point at $\zeta = -1$. At some critical parameter $\zeta = \zeta_{h1} < -1$, the outer island becomes too small to contain the beam and then the beam size will decrease suddenly. On the other hand, when the tune is ramped such that the parameter $\zeta \to -1_-$ from below, the beam size will remain small until the inner island is too small to contain the bunch at $\zeta = \zeta_{h2} < -1$. Above ζ_{h2}, beam particles in the bunch may execute transient betatron oscillations about the outer SFP. This will result in a larger beam size than that of the downramp measurements. This effect depends on the radiation damping rate and the ramping rate as discussed earlier. The hysteresis phenomena can be measured when the condition $|\zeta_{h1} - \zeta_{h2}| \gg 1$ is satisfied.

Alternatively, one can also measure the sharp transition edge and the slope of the beam size increase at the first bifurcation point $\zeta_{b1} = 1$ to determine two parameters of the SBR Hamiltonian. Measurements of other machine parameters, such as α_{xx}, β_x, etc., are needed to determine the Hamiltonian completely.

C. The $3\nu_x \pm m_s Q_s = \ell$ resonances

The Hamiltonian near the third order SBR can be expressed as

$$H = \nu_x I_x + \tfrac{1}{2}\alpha_{xx} I_x^2 - \frac{\eta}{|\eta|}(Q_s I_s + \tfrac{1}{2}\alpha_{ss} I_s^2) + \tilde{g} I_x^{3/2} \cos(3\psi_x + m_s\psi_s - \ell\theta + \gamma). \quad (33)$$

Using the generating function

$$F_2 = \left(\psi_x + \frac{m_s}{3}\psi_s - \frac{\ell}{3}\theta + \frac{\gamma}{3}\right) I_1 + \psi_s I_2,$$

the Hamiltonian in the resonance rotating frame becomes $H = H_1(I_1, \psi_1, I_2) + H_2(I_2)$, with $H_2(I_2) = -\frac{\eta}{|\eta|}(Q_s I_2 + \frac{1}{2}\alpha_{ss} I_2^2)$ and

$$H_1 = \delta_1 I_1 + \frac{1}{2}\alpha_1 I_1^2 + \tilde{g} I_1^{3/2} \cos 3\psi_1. \quad (34)$$

Here $\delta_1 = \nu_x - \frac{\eta}{|\eta|}\frac{m_s}{3}(Q_s + \alpha_{ss} I_2) - \frac{\ell}{3}$ is the resonance proximity parameter and $\alpha_1 = \alpha_{xx} - \frac{\eta}{|\eta|}\frac{m_s^2}{9}\alpha_{ss}$ is the effective resonance detuning parameter. Hamilton's equations of motion are given by

$$\dot{\psi}_1 = \delta_1 + \alpha_1 I_1 + \frac{3}{2}\tilde{g} I_1^{1/2} \cos 3\psi_1, \quad \dot{I}_1 = 3\tilde{g} I_1^{3/2} \sin 3\psi_1. \quad (35)$$

The equation for fixed points of the Hamiltonian is given by

$$w^2 + \frac{3}{2} b w + a = 0, \quad (36)$$

with

$$w = I_1^{1/2} \cos 3\psi_1 \quad (\sin 3\psi_1 = 0), \quad b = \frac{\delta_1}{\alpha_1}, \quad a = \frac{\tilde{g}}{\alpha_1}.$$

The solutions are given by

$$I_{1,\rm SFP}^{\frac{1}{2}} = \begin{cases} 0 & \text{if } b > (\frac{3}{4}a)^2 \ , b < 0 \\ \frac{3}{4}|a| + \sqrt{(\frac{3}{4}a)^2 - b} & \text{if } (\frac{3}{4}a)^2 \geq b, \end{cases}$$

$$I_{1,\rm UFP}^{\frac{1}{2}} = \left|\tfrac{3}{4}|a| - \sqrt{(\tfrac{3}{4}a)^2 - b}\right| \quad \text{if } (\tfrac{3}{4}a)^2 \geq b.$$

Figure 3 shows fixed points $\frac{1}{|a|}\sqrt{I_{1,\rm FP}}$ as a function of $\frac{b}{|a|^2}$. Note here that the resonance islands bifurcate at $b = \frac{9}{16}|a|^2$ and 0. At a sufficiently small sideband resonance strength, which yields $I_{1,\rm SFP} \approx I_{x,\rm rms}$, the beam will also split into three or four pieces. Such sideband resonances may also display hysteresis phenomena.

D. Comments on 3D synchrotron resonances

When a 3D synchrotron sideband resonance $m_x\nu_x + m_z\nu_z - \frac{\eta}{|\eta|}m_s Q_s = \ell$ is encountered, the Hamiltonian can be approximated by

$$H = H_0(I_x, I_z, I_s) + \tilde{g} I_x^{\frac{|m_x|}{2}} I_z^{\frac{|m_x|}{2}} \cos(m_x\psi_x + m_z\psi_z + m_s\psi_s - \ell\theta + \gamma). \quad (37)$$

Using the generating function

$$F_2 = \left(\psi_x + \frac{m_z}{m_x}\psi_z + \frac{m_s}{m_x}\psi_s - \frac{\ell}{m_x}\theta + \frac{\gamma}{m_x}\right) I_1 + \psi_z I_2 + \psi_s I_3,$$

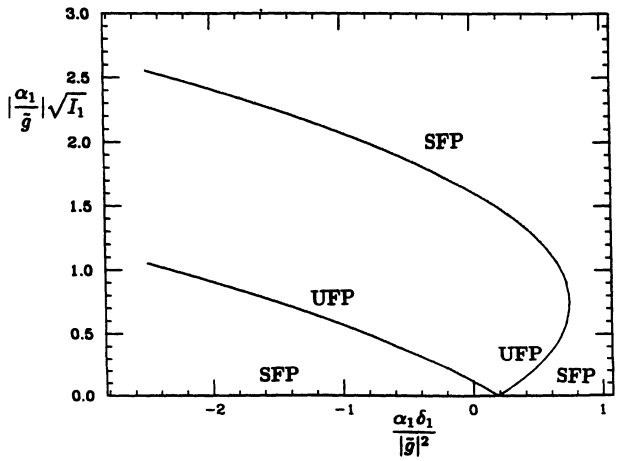

FIG. 3. The square root of the actions of SFPs and UFPs divided by a normalized resonance strength for the third order SBR are plotted as a function of the normalized resonance proximity parameter.

we obtain $I_x = I_1$, $I_z = \frac{m_z}{m_x} I_1 + I_2$, and $I_s = \frac{m_s}{m_x} I_1 + I_3$. The Hamiltonian in the resonance rotating frame becomes $H = H_1(I_1, \psi_1, I_2, I_3) + H_2(I_2) + H_3(I_3)$, with $H_2(I_2) = \nu_z I_2^2 + \frac{1}{2}\alpha_{zz} I_2^2$, $H_3(I_3) = -\frac{\eta}{|\eta|}(Q_s I_3 + \frac{1}{2}\alpha_{ss} I_3^2)$ and

$$H_1 = \delta_1 I_1 + \frac{1}{2}\alpha_1 I_1^2 + \tilde{g} I_1^{\frac{|m_x|}{2}} \left(I_2 + \frac{m_z}{m_x} I_1\right)^{\frac{|m_z|}{2}} \cos m_x \psi_1. \tag{38}$$

Here $\delta_1 = (\nu_x + \alpha_{xz} I_2) + \frac{m_z}{m_x}(\nu_z + \alpha_{xz} I_2) - \frac{\eta}{|\eta|}\frac{m_s}{m_x}(Q_s + \alpha_{ss} I_3) - \frac{\ell}{m_x}$ is the resonance proximity parameter and $\alpha_1 = \alpha_{xx} + 2\frac{m_z}{m_x}\alpha_{xz} + \frac{m_z^2}{m_x^2}\alpha_{zz} - \frac{\eta}{|\eta|}\frac{m_s^2}{m_x^2}\alpha_{ss}$ is the effective resonance detuning parameter.

The Poincaré surface of section of Eq. (38) for 3D synchrotron resonances resembles that of 2D resonances [20]. Without detailed analyses of the Hamiltonian H_1 in resonance rotating frame, observations pertinent to beam stability can be stated as follows. Since I_3 is invariant and $I_s \gg I_{x,z}$, the longitudinal action works as a reservoir in the dynamics of particle motion. Because I_2 is conserved, the transverse amplitude growth will be much larger for the transverse sum resonance sidebands. The transverse growth will be finite for sidebands of transverse difference resonances, where $\frac{m_x}{\beta_x}\sigma_x^2 - \frac{m_z}{\beta_z}\sigma_z^2$ is invariant across the resonance. Experimental observations in LEP showed that $\sigma_x^2 + \sigma_z^2$ was indeed invariant across the $\nu_x - \nu_z + Q_s = \ell$ resonance [9]. It remains to be confirmed that $\beta_x \approx \beta_z$ at the beam profile measurement location because the proper invariant for $\nu_x - \nu_z + Q_s = \ell$ SBR is $\frac{\sigma_x^2}{\beta_x} + \frac{\sigma_z^2}{\beta_z}$. To achieve further detailed understanding of the 3D resonance, measurements of Poincaré maps are essential.

IV. CONCLUSION

The Hamiltonian for the synchro-betatron coupling was discussed in the action-angle variables conforming with the transverse actions. The nonlinear detuning parameters in the synchrotron phase space are found to be small in comparison with that of betatron detuning parameters due to octupoles and sextupoles. Because of a large ratio between the longitudinal and the transverse actions, particle loss via transverse phase space will occur near a SBR, where the dependence of the stop band width on the resonance strength and the nonlinear detuning parameters are also discussed. Because of synchrotron radiation damping, the beam bunch may split into beamlets converging toward SFPs of the Hamiltonian flow. These beamlets are orbiting in the betatron phase space at the tune of $\nu_x \pm \frac{m_s}{m_x} Q_s - \frac{\ell}{m_x}$. A high resolution fast timing profile monitor may be used to measure these stable fixed points (attractors), which may also exhibit hysteresis phenomena. However, it is worth pointing out that a beam bunch consists of particles with different synchrotron and betatron phases. Therefore "a stable island" is actually a ring of islands in the betatron phase space. It may be difficult to resolve the ring of beamlets. A better experiment would require synchrotron and betatron phase space tracking following a coherent synchro-betatron excitation to a beam bunch with small phase space area (a macroparticle).

Measurement of SFPs of the Hamiltonian can be used to determine the SBR Hamiltonian. The ramped tune measurements in LEP was used as an illustrative example. The parameters of a SBR Hamiltonian can be derived from the experimental hysteresis curves. Once the resonance parameters are obtained, one may design a SBR corrector to cancel the SBR harmonic near the operation tunes.

We have discussed mainly single particle dynamics near SBRs of low order betatron sideband synchrotron resonances. When beam-beam interactions [13,14] are included, high order betatron sideband SBRs have been observed [3]. The nonlinear detuning model used in this paper should be modified to reflect the nonlinearities of the beam-beam interaction. More recently, there are many experimental observations on the 3D $m_x\nu_x + m_z\nu_z + m_s Q_s = \ell$ resonances [7,9]. Further studies on these resonances may be important for future high luminosity colliders.

ACKNOWLEDGMENTS

I thank Dr. R. Baartman for helpful comments and Dr. S. Myers for his permission to publish some of his experimental data prior to his publication. This work is supported in part by grants from the NSF, No. PHY-9221402, and the U.S. DOE, No. DE-FG02-93ER40801

APPENDIX A: NONLINEAR DETUNING OF SYNCHROTRON MOTION

The unperturbed Hamiltonian for the synchrotron motion in the conjugate phase space variables $(\frac{R}{h}\phi, -\frac{\Delta p}{p_0})$ is given by

$$H_s = -\frac{1}{2}\eta R\left(\frac{\Delta p}{p_0}\right)^2 - \frac{\nu_s^2 R}{h^2|\eta|}[\cos(\phi + \phi_s) - \cos\phi_s + \phi\sin\phi_s], \tag{A1}$$

where $\nu_s = \sqrt{\frac{h|\eta|eV}{2\pi\beta^2 E}}$ is the synchrotron tune of a stationary bucket at small amplitudes. Hamilton's equations are given by

$$\dot{\phi} = h\eta\frac{\Delta p}{p_0}, \quad \frac{\dot{\Delta p}}{p_0} = \frac{\nu_s^2}{h|\eta|}[\sin(\phi + \phi_s) - \sin\phi_s].$$

The action for a torus $H_s = E_s$ is given by

$$I_s = \frac{1}{2\pi}\frac{R}{h}\oint \frac{\Delta p}{p_0} d\phi = 4.771 \times 10^4 \frac{[\mathcal{A}\ \text{eV s}]}{\beta[E\ \text{GeV}]}\mu\text{m}, \tag{A2}$$

where synchrotron tune is given by $\frac{dE_s}{dI_s}$ and $\mathcal{A}$ is the area in the conjugate phase space variables $(\phi, -\frac{\Delta E}{\omega_{\text{rf}}})$. The action varies from 0 to a maximum value given by

$\hat{I}_s = \frac{16}{2\pi}\frac{\nu_s R}{h^2|\eta|}\alpha(\phi_s)$, where $\alpha(\phi_s) \approx \frac{1-\sin\phi_s}{1+\sin\phi_s}$ is the running bucket reduction factor.

Let $Q_s = \nu_s\sqrt{|\cos\phi_s|}$ be the synchrotron tune of the running bucket at small amplitude. The solution of Hamilton's equations in the first order perturbation theory is given by

$$\phi = \sqrt{\frac{2I_s h^2|\eta|}{RQ_s}}\cos\psi_s, \quad \frac{\Delta p}{p_0} = \sqrt{\frac{2I_s Q_s}{|\eta|R}}\sin\psi_s. \quad \text{(A3)}$$

The nonlinear detuning term can be obtained perturbatively by substituting the first order solution into the Hamiltonian and performing canonical perturbation calculations. The result is given by

$$H_s = -\frac{\eta}{|\eta|}(Q_s I_s + \tfrac{1}{2}\alpha_{ss}I_s^2 + \cdots), \quad \text{(A4)}$$

with

$$\alpha_{ss} = -\frac{h^2|\eta|}{8R}(1 + \tfrac{5}{3}\tan^2\phi_s).$$

The synchrotron detuning parameters α_{ss} for some storage rings are listed in Table I. These nonlinear detuning parameters are found to be of the order of -10 m^{-1}, which is small in comparison with that of the transverse nonlinear detuning parameters α_{xx}, etc., which are of the order of $10^3 - 10^4$ m^{-1} for high energy storage rings.

The conjugate angle variable ψ_s can be obtained from the generating function

$$F_2(\phi, I_s) = -\int_{\hat{\phi}}^{\phi}\left(\frac{\Delta p}{p_0}\right)d\phi',$$

with

$$\psi_s(\phi) = \frac{\partial F_2}{\partial I_s} = -\int_{\hat{\phi}}^{\phi}\frac{\partial(\frac{\Delta p}{p_0})}{\partial I_s}d\phi'. \quad \text{(A5)}$$

Thus the synchrotron phase integral of Eq. (8) can be transformed into an integral over ϕ variable [21]. Making a smooth approximation for the synchrotron motion, the evaluation of the SBR strength is reduced to the calculation of the following integrals:

$$\oint \cos(\phi+\phi_s)e^{im\psi_s(\phi)}d\psi_s,$$

$$\oint \sin(\phi+\phi_s)e^{im\psi_s(\phi)}d\psi_s,$$

$$\oint \phi^n e^{im\psi_s(\phi)}d\psi_s,$$

etc. These integrals can be integrated by using the coordinate transformation of Eq. (A5).

APPENDIX B: SCALING PROPERTIES OF THE ACTION VARIABLES IN SYNCHROTRONS

The emittance of the electron beam in an isomagnetic storage ring is given by

$$\epsilon_x = C_q\frac{\gamma^2\langle\mathcal{H}\rangle}{j_x\rho} = FC_q\frac{\gamma^2\theta_d^3}{j_x}, \quad \text{(B1)}$$

where $C_q = 3.84\times10^{-13}$ m, ρ is the bending radius, and j_x is the damping partition number in the horizontal phase space. The average of the dispersion action is given by $\langle\mathcal{H}\rangle = F\rho\theta_d^3$, where F is a scaling constant and θ_d is the bending angle of dipole(s) in a half cell. For a lattice with periodic focusing and defocusing (FODO) cells, $F \approx 4\frac{1-0.75\sin^2\frac{\Phi}{2}}{\sin^2\frac{\Phi}{2}\sin\Phi}$, where Φ is the phase advance of a FODO cell, and for the minimum emittance double bend achromatic (DBA) lattice, $F = \frac{1}{4\sqrt{15}}$.

The longitudinal action is given by

$$I_s = \frac{1}{2\pi}\frac{R}{h}\pi\left(\frac{\Delta E}{\beta^2 E_0}\right)_{\rm rms}(\Delta\phi)_{\rm rms} = \frac{R|\eta|}{2\nu_s}C_q\frac{\gamma^2}{\rho j_\epsilon}, \quad \text{(B2)}$$

where j_ϵ is the damping partition number in synchrotron phase space. Note here that the longitudinal action is inversely proportional to the synchrotron tune. For a DBA lattice, the momentum compaction factor $\alpha = \frac{1}{6}\frac{\rho\theta_d^2}{R}$. Thus the ratio of the longitudinal action to that of the horizontal one is

$$\frac{I_s}{I_x} \approx 8.2M\frac{1}{4\sqrt{15}F}\frac{0.05}{\nu_s}, \quad \text{(B3)}$$

where M is the number of superperiods for the double bend achromat. Note here that the ratio is independent of energy and is inversely proportional to ν_s. The ratio increases with the number of cells. A similar conclusion can be reached for a lattice with FODO cells. The damping rings of future linear colliders achieve their small emittance by using many FODO cells with small θ_d and employing high betatron phase advance in each FODO cell. The ratio $\frac{I_s}{I_x}$ is about 3×10^3.

For proton storage rings, a typical rms normalized emittance of a beam is about 4π mm mrad for 10^{11} particles per bunch. Thus the action for an rms particle is about

$$I_x \approx I_z \approx \frac{2}{\beta\gamma} \quad \mu\text{m}.$$

Similarly, the rms longitudinal phase space area is about 0.2 eV s. Thus the rms longitudinal action is given by

$$I_s \approx \frac{1}{\beta\gamma}\times10^4 \quad \mu\text{m}.$$

The ratio $\frac{I_s}{I_x}$ will be about 5×10^3 in all cases.

More recently, many low energy storage rings with electron cooling have been constructed for atomic and nuclear physics research. The longitudinal cooling rate is usually an order of magnitude larger than the transverse cooling rate. Because a low energy beam is usually dominated by the space charge effects, the ratio of rms longitudinal action to the transverse actions are actually of the same order of magnitude. As an example, the rms action of the bunched beam at the Indiana University Cyclotron Facility Cooler was found to be about $I_x = 0.025$ μm at 45 MeV kinetic energy for a beam intensity of about 5×10^8 protons. The corresponding longitudinal action was found to be about $I_s \approx 54$ μm. Thus the ratio is about 2×10^3.

[1] M.C. Crowley-Milling and I.I. Rabinowitz, IEEE Trans. Nucl. Sci. **NS-18**, 1052 (1971).
[2] SPEAR Group, IEEE Trans. Nucl. Sci. **NS-22**, 1366 (1975); A. Chao *et al.*, SLAC Report No. SPEAR-187, 1975 (unpublished).
[3] A. Piwinski and A. Wrulich, DESY Report No. 76/07, 1976 (unpublished); A. Piwinski, IEEE Trans. Nucl. Sci. **NS-24**, 1408 (1977); *Proceedings of the 11th International Conference on High Energy Accelerators* (CERN, Geneva, 1980), p. 754.
[4] N.A. Vinokurov *et al.*, *Proceedings of the 10th International Conference on High Energy Accelerators* (Serpukhov, Provino, 1977), p. 272.
[5] R.M. Sundelin, IEEE Trans. Nucl. Sci. **NS-26**, 3604 (1979).
[6] A. Piwinski, IEEE Trans. Nucl. Sci. **NS-24**, 1408 (1977).
[7] D.H. Rice *et al.*, *Proceedings of the IEEE Particle Accelerator Conference, San Francisco, 1991* (IEEE, New York, 1991).
[8] S. Myers, CERN Report No. 91-08, 1991 (unpublished).
[9] S. Myers, in *Measurements of Synchro-Betatron Resonances at LEP*, Proceedings of the Sixth ICFA Beam Dynamics Workshop on Synchro-Betatron Coupling Resonances, Madeira, Portugal, 1993 (CERN, Geneva, in press).
[10] A. Piwinski, CERN Report No. 87-03, 1987 (unpublished), p. 187.
[11] T. Suzuki, Part. Accel. **18**, 115 (1985); C.J.A. Corsten and H.L. Hagedoorn, Nucl. Instrum. Methods **212**, 37 (1983); for an excellent survey of SBR, see T. Suzuki, Part. Accel. **27**, 163 (1990).
[12] R. Baartman (unpublished).
[13] D.V. Pestrikov, Nucl. Instrum. Methods A **336**, 427 (1993).
[14] K. Hirata, H. Moshammer, and F. Ruggiero, Part. Accel. **40**, 205 (1993).
[15] G. Guignard, CERN Report No. 76-06, 1976 (unpublished).
[16] S.Y. Lee, K.Y. Ng, and D. Trbojevic, Phys. Rev. E **48**, 3040 (1993).
[17] D.A. Goldberg and G.L. Lambertson, in *The Physics of Particle Accelerators*, edited by M. Month and M. Dienes, AIP Conf. Proc. No. 249 (AIP, New York, 1992), p. 537.
[18] H. Huang *et al.*, Phys. Rev. E **48**, 4678 (1993); M. Ellison *et al.*, Phys. Rev. Lett. **70**, 591 (1993); M. Syphers *et al.*, *ibid.* **71**, 719 (1993); Y. Wang *et al.*, Phys. Rev. E **49**, 1610 (1994).
[19] D. Li *et al.*, Phys. Rev. E **48**, R1638 (1993).
[20] J.Y. Liu *et al.*, Phys. Rev. E **49**, 2347 (1994).
[21] S.Y. Lee *et al.*, Phys. Rev. E **49**, 5717 (1994).